Prediction of the effects of size and morphology on the structure of water around hematite nanoparticles

Dino Spagnoli [1, 2], Benjamin Gilbert [2], Glenn A. Waychunas [2], and Jillian F. Banfield [1, 2]

1. Department of Earth and Planetary Sciences, University of California-Berkeley, Berkeley, California, 94720, USA
2. Earth Science Division, Lawrence Berkeley National Laboratory, Berkeley, California, 94720, USA

April2009

Abstract

Compared with macroscopic surfaces, the structure of water around nanoparticles is difficult to probe directly. We used molecular dynamics simulations to investigate the effects of particle size and morphology on the time-averaged structure and the dynamics of water molecules around two sizes of hematite (□-Fe_2O_3) nanoparticles. Interrogation of the simulations via atomic density maps, radial distribution functions and bound water residence times provide insight into the relationships between particle size and morphology and the behavior of interfacial water. Both 1.6 nm and 2.7 nm particles are predicted to cause the formation of ordered water regions close to the nanoparticle surface, but the extent of localization and ordering, the connectivity between regions of bound water, and the rates of molecular exchange between inner and outer regions are all affected by particle size and morphology. These findings are anticipated to be relevant to understanding the rates of interfacial processes involving water exchange and the transport of aqueous ions to surface sites.

Introduction

The interactions between water and mineral surfaces are crucial for stabilizing surface structures (ZHANG et al., 2003) and mediating interfacial adsorption reactions of aqueous ions (BROWN, 2001; KERISIT and PARKER, 2004b). Nanoscale minerals, such as hematite (□-Fe_2O_3), are extremely common natural products of biomineralisation (FOWLER et al., 1999) and chemical weathering reactions (GILBERT and BANFIELD, 2005). Although frequently a minority fraction, mineral nanoparticles can have a profound impact on their environment (GILBERT and BANFIELD, 2005), having high surface areas and hence high reactivity and total energy relative to macroscopic minerals. Hematite, like the other iron oxide minerals, is of particular interest because its properties at different sizes indicate a wide range of geochemical reactivity (MADDEN et al., 2006). This includes adsorption of ions from solution, such as phosphates (WAYCHUNAS et al., 2005b) and arsenates (WAYCHUNAS et al., 2005a), photochemical reduction in aqueous solution (SHERMAN, 2005), and heterogeneous catalysis (FENG et al., 2004).

Experimental studies on the mineral-water interface have received a great deal of research attention due to the fact that water often forms an ordered structure above macroscale mineral surfaces. Highly ordered water structure has been observed experimentally on a wide range of minerals including calcite ($CaCO_3$) (GEISSBUHLER et al., 2004), barite ($BaSO_4$) (FENTER et al., 2001), orthoclase ($KAlSi_3O_8$) (FENTER et al., 2003), hematite (TANWAR et al., 2007; TRAINOR et al., 2004) and alumina (□-Al_2O_3) (ZHANG et al., 2008). To gain added insight into this ordered structure, computer simulations provide a complementary tool for investigating this interface. Molecular

dynamics (MD) simulations on the calcite water interface (KERISIT and PARKER, 2004a; KERISIT and PARKER, 2004b) are in very good agreement with the distances of the first two layers of water using *in situ* specular and non-specular X-ray scattering measurements for bulk surfaces (GEISSBUHLER et al., 2004). MD studies of hematite predict water molecules at three distinct distances, 0.19, 0.23 and 0.27 nm, above the (01.2) surface and two distinct distances, 0.24 nm and 0.32 nm, above the (00.1) surface (KERISIT et al., 2005). The first layer above (00.1) is formed by water molecules bonded to hydroxyl groups, whereas the second consists of water molecules interacting with both surface hydroxyls and iron atoms. The structure of the hydroxylated hematite (01.2) surface prepared via wet chemical and mechanical polishing (CMP) procedure was determined using X-ray crystal truncation rod (CTR) diffraction (TANWAR et al., 2007). Comparison of the experimentally determined surface model with density functional theory calculations showed that the hydroxylated CMP-prepared surface differs from an ideal stoichiometric termination due to vacancies of the near surface Fe sites. However, the first layer of water that fitted the CTR data best had a distance of 0.22 nm above the surface, which is relatively close to the results in the MD simulations.

Although the work above involves systems periodic in two dimensions, there are a few examples in the literature of the mineral-water interface involving nanoparticles. Rustad and Felmy used MD to investigate the influence of edge sites on the protonation of goethite nanoparticles with dimensions less than 10 nm (RUSTAD and FELMY, 2005). They predicted that proton accumulation at the surfaces of nanoparticles differs significantly from that on flat surfaces, an effect that they attributed to edge sites. Using both experimental and computational methods, water has been seen to have a stabilizing

effect on the structure of zinc sulfide nanoparticles (ZHANG et al., 2003) and further studies have shown that ZnS nanoparticles can absorb more water molecules per unit surface area compared with bulk ZnS crystals due to increased curvature (ZHANG et al., 2007). Investigations into the water interface with anatase and rutile (TiO_2) (KOPARDE and CUMMINGS, 2007) and calcite (COOKE and ELLIOTT, 2007) nanoparticles predicted two or more hydration layers.

Accurate molecular-scale depictions of interfaces are crucial for determining the physical and chemical constraints on the rates and mechanisms of surface chemical processes such as ion adsorption and mineral dissolution. As discussed above, the nanoparticle-mineral interface has a governing role in many important geochemical processes and atomistic simulations are an increasingly reliable approach for predicting the interfacial structure and properties. In this study we simulated the structure of water around a 2.7 nm faceted, a 2.6 nm spherical and a 1.6 nm nanoparticle and used MD simulations to investigate the structure of water around these hematite nanoparticles and predict important size and shape effects on the extent of water layering and mobility at nanoparticles surfaces.

Methods

All simulations in this work are based on the Born model of solids (BORN and HUANG, 1954), in which the interactions between the atoms of a system are divided into long-range electrostatic interactions and short-range forces. The short-range forces are

described with parameterized functions that include the electron cloud repulsion and the van der Waals attraction forces. The parameters used to model hematite and its interactions with water were based on the potentials developed by Lewis and Catlow (LEWIS and CATLOW, 1985), where the oxygen-oxygen interactions were taken from the work of Catlow (CATLOW et al., 1977). The potential parameters of Baram and Parker (BARAM and PARKER, 1996) were used to model the hydroxyl ion. The potential parameters used to describe the intra- and intermolecular interactions were those of de Leeuw and Parker (DE LEEUW and PARKER, 1998) with the modified hydrogen bond potential of Kerisit and Parker (KERISIT and PARKER, 2004b). These potentials parameters also employ a simple mechanical shell model that was introduced by Dick and Overhauser (DICK and OVERHAUSER, 1958) to account for the ionic polarizability. In our simulations, the cation polarizability was assumed to be negligible and hence the shell model was only used to simulate oxygen ions. The potential parameters are well established and have been used to describe the bulk (COOKE et al., 2003), surface (COOKE et al., 2004) and interfacial (SPAGNOLI et al., 2006a) properties of water and hematite. The water model predicts values for diffusion coefficients, coordination numbers and interaction energies measured experimentally (KERISIT and PARKER, 2004b), which are important when investigating transport properties in interfacial regions. In a recent paper using the same hematite-water potential, the hydrated and hydroxylated surface energies of different hematite surfaces were calculated (DE LEEUW and COOPER, 2007). The calculated surface energies agree well with surface energies from calorimetry experiments (NAVROTSKY et al., 2008).Consequently, the de Leeuw and Parker water model is suitable for the analysis performed here.

All MD simulations were performed using the DL_POLY (SMITH and FORESTER, 1996) computer code. The simulations were initially energy minimized at zero Kelvin using the NVE ensemble (constant number of particles, constant volume and constant energy) for 400 ps. These MD simulations at close to zero Kelvin enable the particle to relax and allow the system to represent the energy at a more optimum value. After 400 ps energy fluctuations of the system drop to ~0.002 eV. The final configuration was then run for a further nanosecond, during which the trajectories were generated in the NPT ensemble (constant number of particles, constant pressure and constant temperature) by means of the Verlet leapfrog algorithm (HOCKNEY, 1970; VERLET, 1967) The time step was 0.2 fs and the temperature was kept constant at 300 K by the Nosé-Hoover thermostat (HOOVER, 1985). The shells were given a small mass of 0.2 a.u. following the approach introduced by Mitchell and Fincham (MITCHELL and FINCHAM, 1993). The electrostatic interactions were calculated using the Ewald summation scheme (EWALD, 1921). All simulations were run for an equilibration period of 200 ps and then run for a further 1 ns, where all data was analyzed. A cut-off of 1.5 nm was used in all simulations.

Simulation Set-up and Analysis

Nanoparticle Morphology

Nanoparticles was constructed using the METADISE code version 5.26 (WATSON et al., 1996), which uses Wulff constructions (WULFF, 1901) to predict the morphology. This approach follows the theory of Gibbs to generate the lowest total surface energy

morphology from facets that may each have different surface energies. The surface energy, □, is defined as the energy per unit area required to create the surface from bulk material, so that:

$$\gamma = \frac{U_s - U_b}{A} \tag{1}$$

where U_s refers to the energy of the block with the created surface and U_b refers to the energy of the bulk material prior to cutting and normalized so that the same number of atoms is present in both blocks. A is the surface area. The surface energies of the hematite surfaces were taken from a previous study using the method described above (KERISIT et al., 2005). For a crystal consisting of a given number of atoms, the equilibrium shape is one that minimizes the surface energy. In 2 dimensions for a polar coordinate system, a vector is drawn parallel to the normal of the surface and with length proportional to the energy of the surface. At the endpoint of the vector a tangent line is drawn. If repeated for all surfaces the tangent lines limit the equilibrium shape. If a particular surface has a high energy, it will not be present in the final construction. The constructions in 3 dimension are in principle the same except a spherical coordinate system is used and at the end of the vectors a tangent plane is drawn. This method can be used to make mineral nanoparticles of any shape or size (COOKE and ELLIOTT, 2007; MARTIN et al., 2006). In the simulations described in this work the initial nanoparticles were bounded by (0.12) unless otherwise stated.

Surface Protonation

Uncertainty surrounding the heterogeneity of proton speciation is one of the major challenges in realistic thermodynamic representation of oxide surfaces (FELMY and RUSTAD, 1998; RUSTAD et al., 1996). This presents a particular challenge for simulations of metal oxide nanoparticles that can possess numerous distinct acidic surface sites. Despite some progress in first principle calculations of pKa values for acidic oxygen sites on surfaces (AQUINO et al., 2008; BICKMORE et al., 2006), acid-base phenomena cannot easily be modeled in MD simulations. In most molecular simulations, including the present work, proton bonding is fixed throughout the run, and thus proton speciation cannot be predicted but must be imposed at the beginning. We developed a semi-empirical method to generate hematite nanoparticles with realistic surface protonation by developing criteria for determining both the degree and location of protonated sites. First, we imposed an effective simulation pH by adding protons until the surface charge density agreed with empirical data from potentiometric titration on hematite powder (SCHUDEL et al., 1997). Second, we determined the location of the protons according to the following procedure. Iron sites coordinated to fewer than 3 structural oxygen atoms were removed, then remaining iron atoms were surrounded by additional oxygens to give the 6-fold coordination expected due to water dissociation at reactive cation sites (RUSTAD et al., 1999). The resulting model nanoparticle possessed only fully coordinated iron sites, with several distinct acidic oxygen sites including iron sites with 1 – 3 bound surface (singly coordinated) oxygen atoms (ηO groups), and two- and three-coordinated oxygen sites (μ_2O and μ_3O sites). Surface oxygen may undergo sequential protonation reactions, so to identify the likely protonation configurations we used a Pauling bond order model (Rustad et al., 1999). Surface sites were protonated as described in Table 1 until the

desired total charge for the nanomaterial was attained. This simple method neglects numerous essential energetic contributions to surface protonation reactions including surface relaxation, solvation and the formation of hydrogen bonding networks across the surface and into the liquid. However, the approach we have developed is consistent with the conclusions made from more sophisticated computer simulations on the most likely sites for proton affinity (RUSTAD et al., 1999). A discussion on the methodology behind protonating the nanoparticle surfaces can be found in the Electronic Annex.

Surface protonated nanoparticles were energy minimized at zero Kelvin and NVE ensemble in DL_POLY 2. The final configuration was then submerged in a box of water. Each nanoparticle was placed in a box big enough so that water at the edge of the simulation cell had the properties of bulk water. A 3-4 nm separation of all nanoparticle surfaces from the box edges was used because layering never extended more than 1 nm from the particle surface. The amount of water added ranged from 2500 to 4800 molecules depending on the size of the simulation cell.

Analysis of the Simulation Results

Radial distribution functions (RDF) are used to describe the structure of hematite nanoparticles and the ordering of water around the particles. RDF is a pair correlation function that describes how, on average, the atoms in a system are radially packed around each other. In a system where there is continual movement of atoms a single snapshot of the system shows only the instantaneous disorder, thus the advantage of RDF is that gives the average structure over a number of configurations. The RDF, g (r), is plotted as a

function of the interatomic separation, r, and peaks along the curve indicate distances at which water molecules pack into 'shells'. Peaks at large distances represent a high degree of ordering (crystalline materials have particularly sharp peaks at large distances because the atoms are strongly confined to their positions). RDFs containing only a fraction of all pair correlations (partial RDFs) are useful for analysis of the form of water layering at surface vs. edge vs. corner sites on nanoparticles.

Residence times indicate how tightly bound a water molecule is to the nanoparticle surface and how long a water molecule will spend in the first hydration shell of the nanoparticle. The residence time is calculated from the residence time correlation function, as defined by Impey et al. (IMPEY et al., 1983). The residence time can be calculated by integration of the residence time correlation. Residence times have been used to describe the dynamics of water around ions (OHTAKI and RADNAI, 1993), surfaces (SPAGNOLI et al., 2006a), and nanoparticles (KERISIT et al., 2005; KOPARDE and CUMMINGS, 2007).

Results and Discussion

Prediction of the structure of hematite and water as a function of size

Two nanoparticles, 1.6 and 2.7 nm in diameter, were placed in a box of water. The four ions in the centre of the nanoparticle were fixed to restrict nanoparticle diffusion while permitting particle structural relaxation and rearrangement of water molecules into the most energetically favorable configurations. To visualize the structure of water

around a nanoparticle in 3 dimensions the water density was evaluated by splitting the simulation cell into 0.3 Å cubic bins. The density was calculated by evaluating the number of times a water molecule passed through a given bin. This approach is similar to the method that was used to illustrate the water density on flat and stepped surfaces of calcite (SPAGNOLI et al., 2006b). We employed two methods to generate viewable 2D images from the 3D structural information: projecting the information from the entire simulation volume onto 2 dimensions (Figs. 1i&ii), and taking cross-sections through the centre of the simulation cell (Figs. 1iii&iv). The blue spots indicate a site occupied by an iron atom and the spot size indicates atom movement due to relaxation and thermal vibrations during the simulation. Both starting configurations of the nanoparticles are crystalline, but during the course of the simulation the 1.6 nm particle structure becomes disordered. The RDF describing interatomic distances between all the iron and oxygen atoms in the hematite crystallites indicates the degree of structural disorder. As shown in the inset to Fig. 2, the RDF between the iron atoms and the oxygen atoms in the 1.6 nm hematite particle is highly disordered compared with that of the larger particle. Although hematite lattice planes can still be discerned in Fig 1iv, the RDF peaks from 0.34 to 0.47 nm are featureless and the particle loses its initial faceted morphology, becoming more spherical. By contrast, the 2.7 nm nanoparticle retains a highly crystalline structure with resolved peaks at all distances in the RDF. The retention of long-range order of crystal structure in larger nanoparticles is a common observation in MD studies (COOKE and ELLIOTT, 2007; MARTIN et al., 2006). There are so few bulk ions relative to surface ions in the 1.6 nm hematite particle that the amount of disorder in the particle is high.

Variations in water density are indicated by color, which ranges from white (no water density) through pink (low water density) to red (high water density). Figures 1.i and 1.ii show that the water adopts an ordered, layered structure near the surfaces of both the 2.7 nm and 1.6 nm nanoparticles. The ordering is greatest at the surface, diminishing with distance until the water is unstructured and indistinguishable from bulk water. At least three water layers are predicted to form at the surfaces of both particles, but the layers are more clearly defined for the 2.7 nm case (Figure 1.iii). We attribute the greater water disorder for the 1.6 nm case to the smaller particle size and loss of crystallinity.

RDFs in Figure 2 show four peaks at 0.22, 0.40, 0.65 and 0.9 nm associated with water layers and tend towards unity, as expected, at greater distances from the surface. The first peak represents the first layer of tightly bound water; its area normalized by the number of surface iron atoms per particle, represents the coordination number of iron by water. Experimental studies have found the first layer of water at 0.27 nm (CATALANO et al., 2007) and 0.22 nm (TANWAR et al., 2007) above the (01.2) hematite surface, which is reasonably close to our simulations and previous MD studies on 2 dimensional surfaces (KERISIT et al., 2005). Direct quantitative comparisons cannot be made between these RDF curves for the two particle sizes because a higher radius of curvature increases the number of water molecules found at a given distance from a surface iron site. Nevertheless, there is a significant difference in the minimum RDF intensity between first and second water layers for the two particle sizes. This minimum indicates an energy cost for water molecules at this position and implies an energy barrier that impedes transfer of water molecules between the first two layers. Consequently, the simulations predict that water exchange rates between the first two layers will be significantly

different for the two nanoparticles studied. To further explore the relationship between particle size and shape and water exchange rates, an additional simulation was performed to predict water structure at the surface of a 2.6 nm spherical nanoparticle.

Prediction of the structure of water as a function of shape and surface site

Figure 3 shows cross-sections through the atomic density maps for the 2.7 nm diameter (01.2) faceted and 2.6 nm spherical hematite nanoparticles. Compared to the 1.6 nm spherical particle shown in Figure 2, both larger particles impose greater ordering on surface water. Interfacial water forms more continuous and extended layers around the faceted 2.7 nm nanoparticle than the spherical 2.6 nm nanoparticle. Numerous isolated patches of bound water develop around the spherical diameter. Taken together, these two observations indicate that surfaces with larger facets or lower curvature are more effective at imparting order to bound water. Furthermore, the faceted particle imposes facets on the surrounding water layers.

We calculated several partial RDF curves between water molecules and specific sites on the surface of the faceted nanoparticle. The crystalline nature of the (01.2) 2.7 nm particle allows us to categorize sites as planar (flat surfaces), corner, or edge. The partial RDF of an iron site on planar (01.2) surfaces (Figure 3b) shows a first peak at 0.22 nm and then from 0.35 nm to 0.61 nm a series of sharp peaks. These peaks indicate a high degree of structural order for water at planar surfaces compared to water in the vicinity of corner or edge sites, or at the surface of a spherical particle. The partial RDF of an iron

site on the disordered 1.6 nm nanoparticle surfaces is similar to that of the corner/edge sites and larger spherical particle.

Strikingly, the partial RDF intensity minimum between the first two water layers at a planar surface reaches zero, but remain non-zero for all other surface sites. Thus, we predict that the rate of movement of water molecules directly between the first two water layers on the side of a faceted nanoparticle will be very slow and water diffusion will occur primarily parallel to the surface. For faceted nanoparticles, exchange of water molecules between the first and second layers should occur primarily at edge or corner sites.

To further analyze the dynamics of water at the nanoparticle surface, we calculated the average velocity of water traveling in two different directions. The average velocity of water traveling perpendicular to the surface is around 60% slower than the average velocity of water traveling parallel to it (Table 2). A related finding from MD studies on large facets on hematite (KERISIT et al., 2005) is that diffusion of water parallel to the surface differs from that normal to the surface. At edge and corner sites, the disruption of the water layer structure permits the transport of molecules between first and second layers. This is consistent with the prediction that the exchange of water molecules between the first two water layers will occur largely at the corner and edge sites.

We compared the structure of water around hematite nanoparticles and a 2 dimensional flat (01.2) hematite surface and calculated the density of water relative to bulk water as a function of perpendicular distance (Figure 4). The (01.2) hematite surface was constructed as reported previously (KERISIT et al., 2005). The hematite slab had a

thickness of 3.4 nm and a surface area of 2.02 x 3.17 nm^2 (Figure 5). Simulations predict that the water adjacent to the surface is highly layered (Figures 4 and 5) The first layer is split into three modes of water adsorption (partly evident in Figure 5), with peaks in the 1 D density plot at 0.18, 0.23 and 0.27 nm from the surface. Due to the highly ordered nature of the flat (01.2) hematite surface there are areas additional layers of high water density (Figure 5) that give rise to peaks in the 1D density plot at 0.46 and 0.74 nm (Figure 4).

The density of water relative to bulk was also calculated for all nanoparticles perpendicular to the surface. In all three cases, the layering is less defined than for the 2 dimensional flat surface, however, the layers are still apparent. For all three nanoparticles, the first two layers of water are centered at 0.21 and 0.45 nm from the surface. For the planar (01.2) surface of the 2.7 nm hematite nanoparticle there is some suggestion of three modes of water adsorption, based on small peaks at 0.18, 0.21 and 0.26 nm. For all three nanoparticles, the densities of the first two water layers (maximum values of 1.30, 1.15 and 1.09 g/cm^3 for the 2.7 nm faceted, 2.6 nm spherical and 1.6 nm disordered nanoparticles respectively) are much lower than for the 2 dimensional flat surface (3.1 g/cm3).

We can use the water density perpendicular to the surface, □, as an approximation for the partition function, to give the free energy difference, □□ for water molecules at different distances from the surface, z, (MARRINK and BERENDSEN, 1994).

$$\Delta A_z = -RT \ln\left(\frac{\rho_z}{\rho_0}\right) \qquad (2)$$

Table 3 shows that the free energy of adsorption (□□ for the three adsorption modes in the first water layer on the (01.2) infinite flat surface is 2 $kJmol^{-1}$ lower than values for nanoparticle surfaces. Although only an estimate, the smaller value on the flat surface indicates higher stabilization of the water layers by the underlying periodic structure.

The dynamics can be further investigated by calculating the residence times of water molecules at different surface sites (Table 4). The calculated residence times do not distinguish between the mobility of water molecules due to exchange between layers (perpendicular to the surface) or to diffusion within a layer (parallel to a surface). Results indicate that the residence times on flat 2D (infinite) surfaces are exceedingly long (as reported by (KERISIT, 2004)), and greatly exceed residence times on any nanoparticle surface considered here.

Water localization is disrupted by the competing effects of underlying hematite layers in different crystallographic orientations. This leads to 'faceting' of water layers around larger non-spherical particles and highly disparate residence times for corner sites, edge sites, and planar surfaces. This finding is consistent with other MD studies of aqueous polynuclear clusters (WANG et al., 2007). The longest residence times occur on the spherical nanoparticle surfaces, where frustration of layers by the underlying curved hematite surfaces leads to strong spatial localization of water molecules (discrete red spots in Figure 3). For the small particle, the result is disordering of water layers and the shortest average residence time.

Conclusions

The MD simulations predict that water close to the surfaces of the hematite nanoparticles forms several ordered layers characterized by much shorter residence times than are predicted for water at planar (infinite) hematite surfaces. As particle size decreases and particles become less crystalline, water layers become less distinct. On the larger faceted particle the extent of ordering increases and the exchange rates for water between layers decreases from corner sites to edges sites to planar surfaces. The average velocity of water is faster parallel compared to perpendicular to water layers. In combination, the results suggest that water moves from the bulk to the surface, and vise versa primarily through the junctions of facets in the solvation layers. Thus, underlying mineral facet junctions could mediate the transport of ions, by creating a mechanism to bypass ordered water regions. In contrast to the extended nanoparticle surfaces, which lead to ordered water layers, curved surfaces create isolated patches in which water may become trapped. Thus, the simulations suggest that the structure and morphology of nanoparticle surfaces contribute to heterogeneity in surface reactivity by affecting the exchange rates of water molecules at mineral surfaces. Moreover, the structure of water could influence nanoparticle reactivity such as crystal growth via oriented aggregation (PENN and BANFIELD, 1998).

Acknowledgements: We thank Prof. Stephen C. Parker for provision of the METADISE code and for useful discussions. We thank Dr Sebastien Kerisit, Dr David J. Cooke, Dr Paolo Raiteri and Prof. William H. Casey for useful discussions. This work was supported with the computer resources provided by the Geochemistry Computer Cluster run by the Scientific Cluster Support group at the Lawrence Berkeley National Laboratory. Funding for this research was supported by the Director, Office of Science, Office of Basic Energy Sciences, Division of Chemical Sciences, Geosciences, and Biosciences, of the U.S. Department of Energy under Contract Numbers. DE-FG02-01ER15218 and DE-AC02-05CH11231.

References

Aquino, A. J. A., Tunega, D., Haberhauer, G., Gerzabek, M. H., and Lischka, H., 2008. Acid-base properties of a goethite surface model: A theoretical view. *Geochim. Cosmochim. Acta* **72**, 3587-3602.

Baram, P. S. and Parker, S. C., 1996. Atomistic simulation of hydroxide ions in inorganic solids. *Philosophical Magazine B-Physics of Condensed Matter Statistical Mechanics Electronic Optical and Magnetic Properties* **73**, 49-58.

Bickmore, B. R., Rosso, K. M., Tadanier, C. J., Bylaska, E. J., and Doud, D., 2006. Bond-valence methods for pK(a) prediction. II. Bond-valence, electrostatic, molecular geometry, and solvation effects. *Geochim. Cosmochim. Acta* **70**, 4057-4071.

Born, M. and Huang, K., 1954. *Dynamical Theory of Crystal Lattices*. Oxford University Press, Oxford.

Brown, G. E., 2001. Surface science - How minerals react with water. *Science* **294**, 67-+.

Catalano, J. G., Fenter, P., and Park, C., 2007. Interfacial water structure on the (012) surface of hematite: Ordering and reactivity in comparison with corundum. *Geochim. Cosmochim. Acta* **71**, 5313-5324.

Catlow, C. R. A., Norgett, M., and Ross, T. A., 1977. Ion transport and interatomic potentials in alkaline-earth-fluoride crystals. *J. Phys. C: Solid St. Phys.* **10**, 1627-1640.

Cooke, D. J. and Elliott, J. A., 2007. Atomistic simulations of calcite nanoparticles and their interaction with water. *J. Chem. Phys.* **127**, 9.

Cooke, D. J., Parker, S. C., and Osguthorpe, D. J., 2003. Calculating the vibrational thermodynamic properties of bulk oxides using lattice dynamics and molecular dynamics. *Phys. Rev. B* **67**.

Cooke, D. J., Redfern, S. E., and Parker, S. C., 2004. Atomistic simulation of the structure and segregation to the (0001) and (01(1)over-bar2) surfaces of Fe2O3. *Phys. Chem. Miner.* **31**, 507-517.

de Leeuw, N. H. and Cooper, T. G., 2007. Surface simulation studies of the hydration of white rust Fe(OH)(2), goethite alpha-FeO(OH) and hematite alpha-Fe2O3. *Geochim. Cosmochim. Acta* **71**, 1655-1673.

de Leeuw, N. H. and Parker, S. C., 1998. Molecular-dynamics simulation of MgO surfaces in liquid water using a shell-model potential for water. *Phys. Rev. B* **58**, 13901-13908.

Dick, A. W. and Overhauser, B. G., 1958. Theory of dielectric constants of alkali halide crystals. *Phys. Rev.* **112**, 90-103.

Ewald, P. P., 1921. Die berechnung optisher und elektostatischer gitterpotentiale. *Annalen der Physik* **64**, 253.

Felmy, A. R. and Rustad, J. R., 1998. Molecular statics calculations of proton binding to goethite surfaces: Thermodynamic modeling of the surface charging and protonation of goethite in aqueous solution. *Geochim. Cosmochim. Acta* **62**, 25-31.

Feng, J. Y., Hu, X. J., and Yue, P. L., 2004. Discoloration and mineralization of orange II using different heterogeneous catalysts containing Fe: A comparative study. *Environmental Science & Technology* **38**, 5773-5778.

Fenter, P., Cheng, L., Park, C., Zhang, Z., and Sturchio, N. C., 2003. Structure of the orthoclase (001)- and (010)-water interfaces by high-resolution X-ray reflectivity. *Geochim. Cosmochim. Acta* **67**, 4267-4275.

Fenter, P., McBride, M. T., Srajer, G., Sturchio, N. C., and Bosbach, D., 2001. Structure of barite (001)- and (210)-water interfaces. *J. Phys. Chem. B* **105**, 8112-8119.

Fowler, T. A., Holmes, P. R., and Crundwell, F. K., 1999. Mechanism of pyrite dissolution in the presence of Thiobacillus ferrooxidans. *Applied and Environmental Microbiology* **65**, 2987-2993.

Geissbuhler, P., Fenter, P., DiMasi, E., Srajer, G., Sorensen, L. B., and Sturchio, N. C., 2004. Three-dimensional structure of the calcite-water interface by surface X-ray scattering. *Surf. Sci.* **573**, 191-203.

Gilbert, B. and Banfield, J. F., 2005. Molecular-scale processes involving nanoparticulate minerals in biogeochemical systems, *Molecular Geomicrobiology*. 109-155

Hockney, R. W., 1970. *The potential calculation and some applications*. Academic Press, New York/London.

Hoover, W. G., 1985. Canonical Dynamics - Equilibrium Phase-Space Distributions. *Phys Rev A* **31**, 1695-1697.

Impey, R. W., Madden, P. A., and McDonald, I. R., 1983. Hydration and Mobility of Ions in Solution. *J. Phys. Chem* **87**, 5071-5083.

Kerisit, S., 2004. Atomistic Simulation of Calcite Surfaces. PhD Thesis, University of Bath.

Kerisit, S., Cooke, D. J., Spagnoli, D., and Parker, S. C., 2005. Molecular dynamics simulations of the interactions between water and inorganic solids. *J. Mater. Chem.* **15**, 1454-1462.

Kerisit, S. and Parker, S. C., 2004a. Free energy of adsorption of water and calcium on the {10(1)over-bar-4} calcite surface. *Chem. Commun.*, 52-53.

Kerisit, S. and Parker, S. C., 2004b. Free Energy of Adsorption of Water and Metal Ions on the {104} Calcite Surface. *J. Am. Chem. Soc.* **126**, 10152 - 10161.

Koparde, V. N. and Cummings, P. T., 2007. Molecular dynamics study of water adsorption on TiO2 nanoparticles. *Journal of Physical Chemistry C* **111**, 6920-6926.

Lewis, G. V. and Catlow, C. R. A., 1985. Potential model for ionic oxides. *J. Phys. C: Solid St. Phys.* **18**, 1149-1161.

Madden, A. S., Hochella, M. F., and Luxton, T. P., 2006. Insights for size-dependent reactivity of hematite nanomineral surfaces through Cu2+ sorption. *Geochim. Cosmochim. Acta* **70**, 4095-4104.

Marrink, S. J. and Berendsen, H. J. C., 1994. Simulation of Water Transport through a Lipid-Membrane. *J. Phys. Chem* **98**, 4155-4168.

Martin, P., Spagnoli, D., Marmier, A., Parker, S. C., Sayle, D. C., and Watson, G. W., 2006. Applications of molecular dynamics DL_POLY codes to interfaces of inorganic materials. *Mol. Simul.* **32**, 1079-1093.

Mitchell, P. J. and Fincham, D., 1993. Shell-Model Simulations by Adiabatic Dynamics. *J. Phys.-Condes. Matter* **5**, 1031-1038.

Navrotsky, A., Mazeina, L., and Majzlan, J., 2008. Size-driven structural and thermodynamic complexity in iron oxides. *Science* **319**, 1635-1638.

Ohtaki, H. and Radnai, T., 1993. Structure and Dynamics of Hydrated Ions. *Chem. Rev.* **93**, 1157-1204.

Penn, R. L. and Banfield, J. F., 1998. Imperfect oriented attachment: Dislocation generation in defect-free nanocrystals. *Science* **281**, 969-971.

Rustad, J. R. and Felmy, A. R., 2005. The influence of edge sites on the development of surface charge on goethite nanoparticles: A molecular dynamics investigation. *Geochim. Cosmochim. Acta* **69**, 1405-1411.

Rustad, J. R., Felmy, A. R., and Hay, B. P., 1996. Molecular statics calculations of proton binding to goethite surfaces: A new approach to estimation of stability constants for multisite surface complexation models. *Geochim. Cosmochim. Acta* **60**, 1563-1576.

Rustad, J. R., Wasserman, E., and Felmy, A. R., 1999. Molecular modeling of the surface charging of hematite - II. Optimal proton distribution and simulation of surface charge versus pH relationships. *Surf. Sci.* **424**, 28-35.

Schudel, M., Behrens, S. H., Holthoff, H., Kretzschmar, R., and Borkovec, M., 1997. Absolute aggregation rate constants of hematite particles in aqueous suspensions: A comparison of two different surface morphologies. *J. Colloid Interface Sci.* **196**, 241-253.

Sherman, D. M., 2005. Electronic structures of iron(III) and manganese(IV) (hydr)oxide minerals: Thermodynamics of photochemical reductive dissolution in aquatic environments. *Geochim. Cosmochim. Acta* **69**, 3249-3255.

Smith, W. and Forester, T. R., 1996. DL_POLY_2.0: A general-purpose parallel molecular dynamics simulation package. *J. Mol. Graph.* **14**, 136-141.

Spagnoli, D., Cooke, D. J., Kerisit, S., and Parker, S. C., 2006a. Molecular dynamics simulations of the interaction between the surfaces of polar solids and aqueous solutions. *J. Mater. Chem.* **16**, 1997-2006.

Spagnoli, D., Kerisit, S., and Parker, S. C., 2006b. Atomistic simulation of the free energies of dissolution of ions from flat and stepped calcite surfaces. *J. Cryst. Growth* **294**, 103-110.

Tanwar, K. S., Lo, C. S., Eng, P. J., Catalano, J. G., Walko, D. A., Brown, G. E., Waychunas, G. A., Chaka, A. M., and Trainor, T. P., 2007. Surface diffraction study of the hydrated hematite (1(1)over-bar-02) surface. *Surf. Sci.* **601**, 460-474.

Trainor, T. P., Chaka, A. M., Eng, P. J., Newville, M., Waychunas, G. A., Catalano, J. G., and Brown, J. G. E., 2004. Structure and reactivity of the hydrated (001) hematite surface. *Surf. Sci.* **573**, 204-224.

Verlet, L., 1967. Computer "Experiments" on Classical Fluids. I. Thermodynamical Properties of Lennard-Jones Molecules. *Phys. Rev. J1 - PR* **159**, 98 LP - 103.

Wang, J. W., Rustad, J. R., and Casey, W. H., 2007. Calculation of water-exchange rates on aqueous polynuclear clusters and at oxide-water interfaces. *Inorg. Chem.* **46**, 2962-2964.

Watson, G. W., Kelsey, E. T., deLeeuw, N. H., Harris, D. J., and Parker, S. C., 1996. Atomistic simulation of dislocations, surfaces and interfaces in MgO. *J. Chem. Soc.-Faraday Trans.* **92**, 433-438.

Waychunas, G., Trainor, T., Eng, P., Catalano, J., Brown, G., Davis, J., Rogers, J., and Bargar, J., 2005a. Surface complexation studied via combined grazing-incidence EXAFS and surface diffraction: arsenate an hematite (0001) and (10-12). *Analytical and Bioanalytical Chemistry* **383**, 12-27.

Waychunas, G. A., Kim, C. S., and Banfield, J. F., 2005b. Nanoparticulate iron oxide minerals in soils and sediments: unique properties and contaminant scavenging mechanisms. *J. Nanopart. Res.* **7**, 409-433.

Wulff, G., 1901. *Kristallogr. Kristallgeom.* **39**, 449.

Zhang, H. Z., Gilbert, B., Huang, F., and Banfield, J. F., 2003. Water-driven structure transformation in nanoparticles at room temperature. *Nature* **424**, 1025-1029.

Zhang, H. Z., Rustad, J. R., and Banfield, J. F., 2007. Interaction between water molecules and zinc sulfide nanoparticles studied by temperature-programmed desorption and molecular dynamics simulations. *J. Phys. Chem. A* **111**, 5008-5014.

Zhang, L., Tian, C., Waychunas, G. A., and Shen, Y. R., 2008. Structures and charging of alpha-alumina (0001)/water interfaces studied by sum-frequency vibrational spectroscopy. *J. Am. Chem. Soc.* **130**, 7686-7694.

Tables

Surface Site	Protonation State(s)	Bond Order	Notes
μ_2OH	Fe_2OH	0	All sites hydroxyl
1 x ηOH	$O_5Fe-OH \Leftrightarrow O_5Fe-OH_2$	-0.5 ⇔ +0.5	50% sites hydroxyl 50% sites water
2 x ηOH	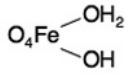	0	One water, one hydroxyl per site
3 x ηOH	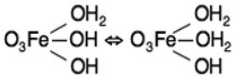	-0.5 ⇔ +0.5	50% sites two waters 50% sites one water
μ_3OH	$Fe_3O \Leftrightarrow Fe_3OH$	-0.5 ⇔ +0.5	Protons added to make up total surface charge

Table 1: Summary of the types of acidic surface sites on the hematite nanoparticles and the protonation strategy based upon calculation of the Pauling bond order.

Surface	Average velocity parallel to the surface (Å/ps)	Average velocity perpendicular to the surface (Å/ps)
1.6 nm particle	1.34±0.3	0.85±0.2
2.7 nm faceted particle	1.35±0.1	0.86±0.1
2.6 nm spherical particle	1.41±0.1	0.89±0.1

Table 2: Average velocity of water traveling parallel and perpendicular to the surface of hematite nanoparticles

Hematite surface type	Free energy difference / $kJmol^{-1}$
Infinite (01.2) Hematite 2D surface	-2.74, -2.18, -2.18
2.7 nm faceted Hematite particle	-0.62
2.6 nm spherical Hematite particle	-0.35
1.6 nm Hematite particle	-0.21

Table 3: Free energy change when a molecule moves from bulk water to flat and curved nanoparticle surfaces

Fe Site	Residence Time (ps)
1.6 nm (01.2) Surface	117.13± 29.13
2.7 nm (01.2) Corner	45.99± 6.93
2.7 nm (01.2) Edge	46.62± 14.19
2.7 nm (01.2) Planar	203.48 ± 14.32
2.7 nm Sphere	327.92± 35.40
(01.2) 2D surface	>1000

Table 4: Residence time of water molecules in the first hydration shell for the planar 2D (infinite) surface, different sites on faceted particles and for sites on spherical, and very small nanoparticles.

Figure Captions

Figure 1: 3 dimensional projection of the water density around 2.7 nm (01.2) (i) and 1.6 nm (01.2) nanoparticles (ii). The cross sections of the water density around the 2.7 nm (iii) and the 1.6 nm (iv) nanoparticles show the extent of the water layering. The blue color indicates an iron site, pink color indicates the area with low water density and red color indicates the area with high water density.

Figure 2: Radial Distribution Function (RDF) between all iron atoms with all the oxygen of the water molecules of 2.7 (black line) and 1.6 nm (red line) (01.2) particles. The arrow indicates the position of the first minimum between the first and second layers of water. Insert is the RDF between iron and oxygen atoms of the 2.7 (black line) and 1.6 nm (red line) hematite particles. The oscillations in the RDF for the larger particle are due to atomic periodicities at larger distances.

Figure 3: a) Cross section of the water density around a 2.7 nm (01.2) faceted and spherical particle. The blue color indicates an iron site, pink color indicates the area with low water density and red color indicates the area with high water density. b) Partial Radial Distribution Function of an iron site on planar surface (black line) and corner/edge surface site (red line) of a 2.7 nm (01.2) particle, an iron site on a spherical surface (blue line) and an iron site on a 1.6 nm disordered particle (green line) with the oxygen of the water molecules.

Figure 4: The density of water relative to bulk for the 2 dimensional flat (01.2) surface (dashed line), the 2.7 nm (01.2) nanoparticle (black line), the 1.6 nm disordered nanoparticle (red line) and 2.6 nm spherical nanoparticle (green line).

Figure 5: A graphical representation of the simulation set-up of the (01.2) hematite 2 dimensional surface (top) and the 3 dimensional projection of the water density, where the blue indicates the Fe sites in the solid, dark red indicates high water density and pink indicates low water density.

Figure 1

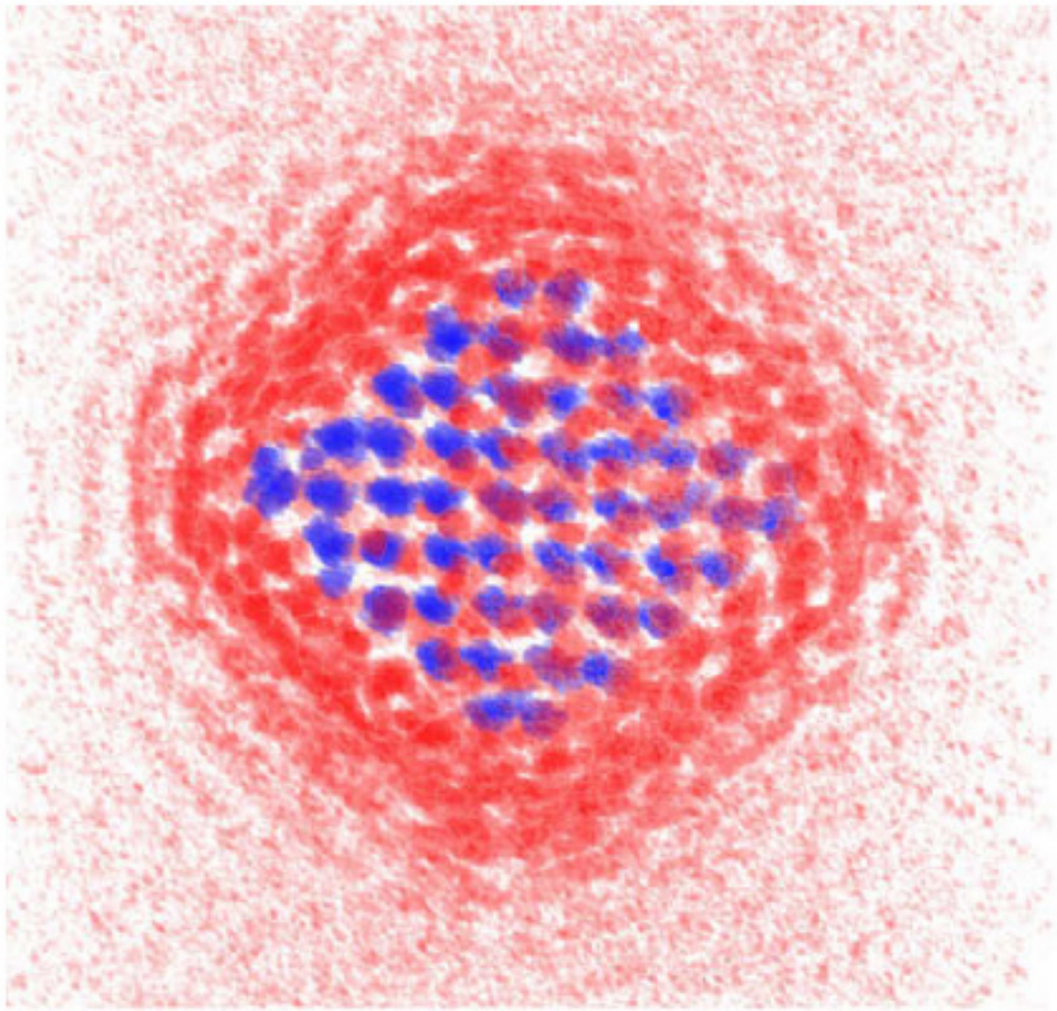

i

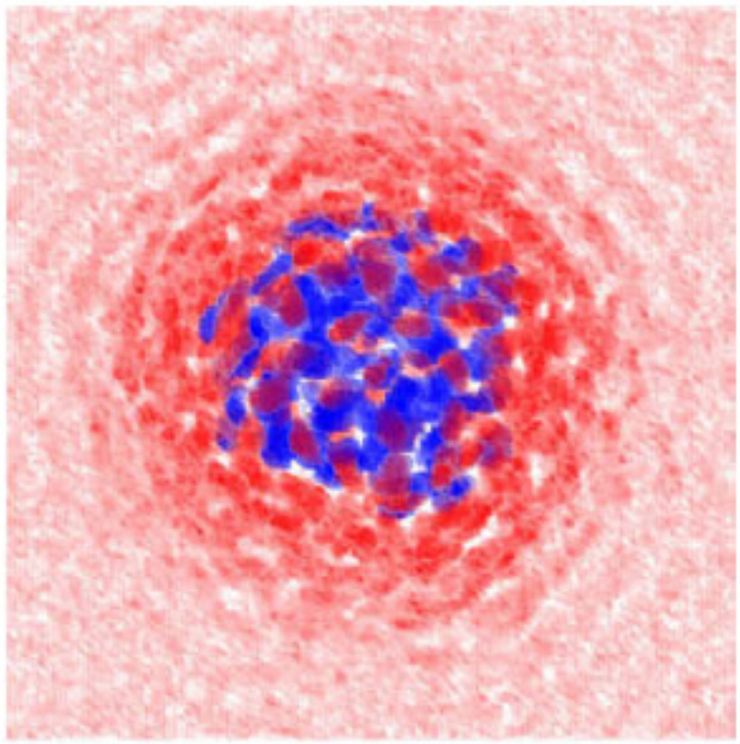

ii

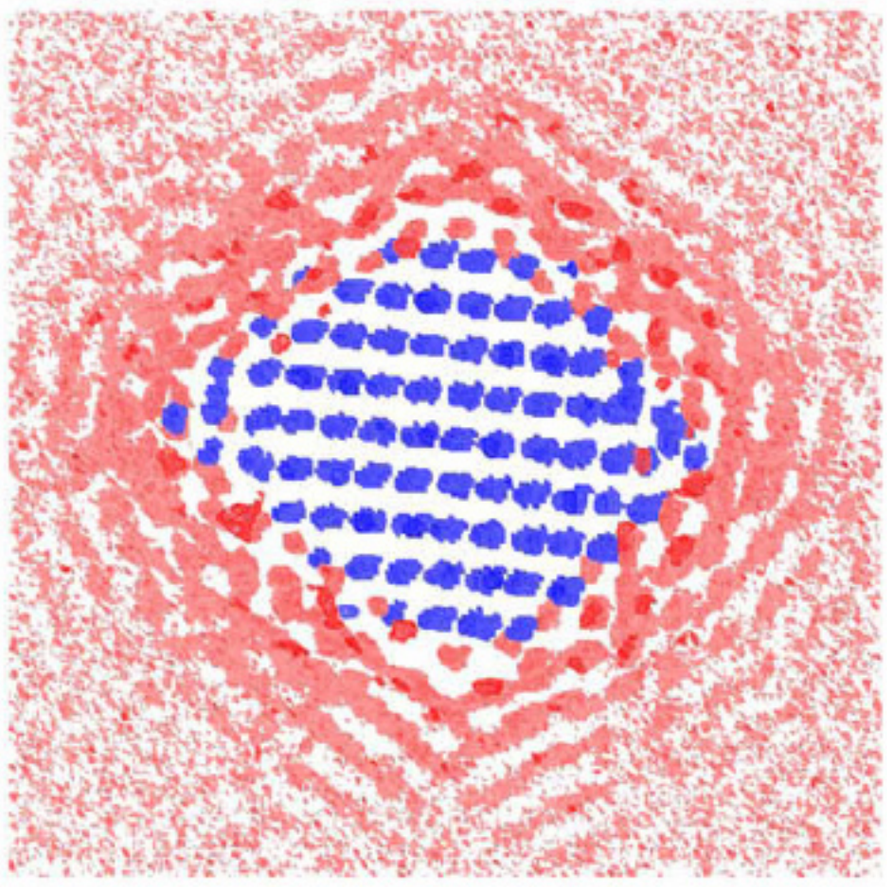

iii

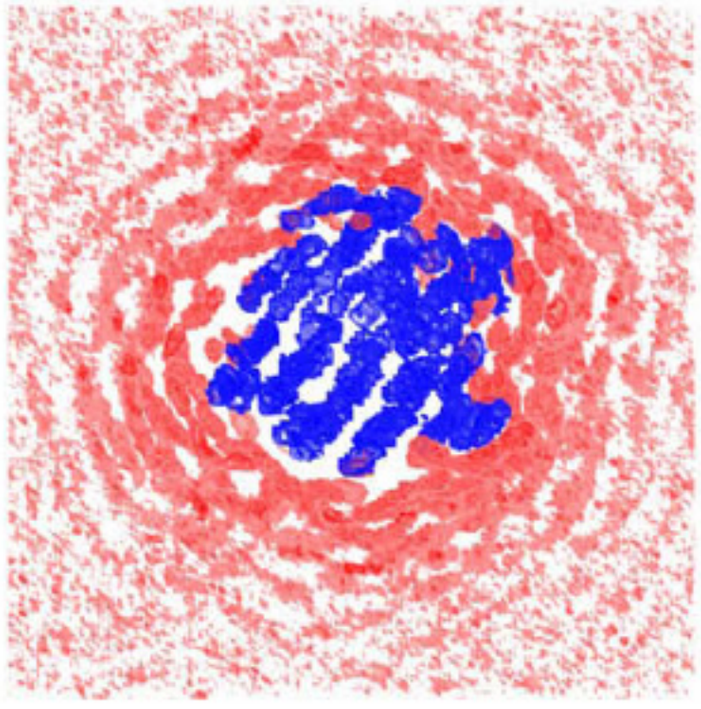

iv

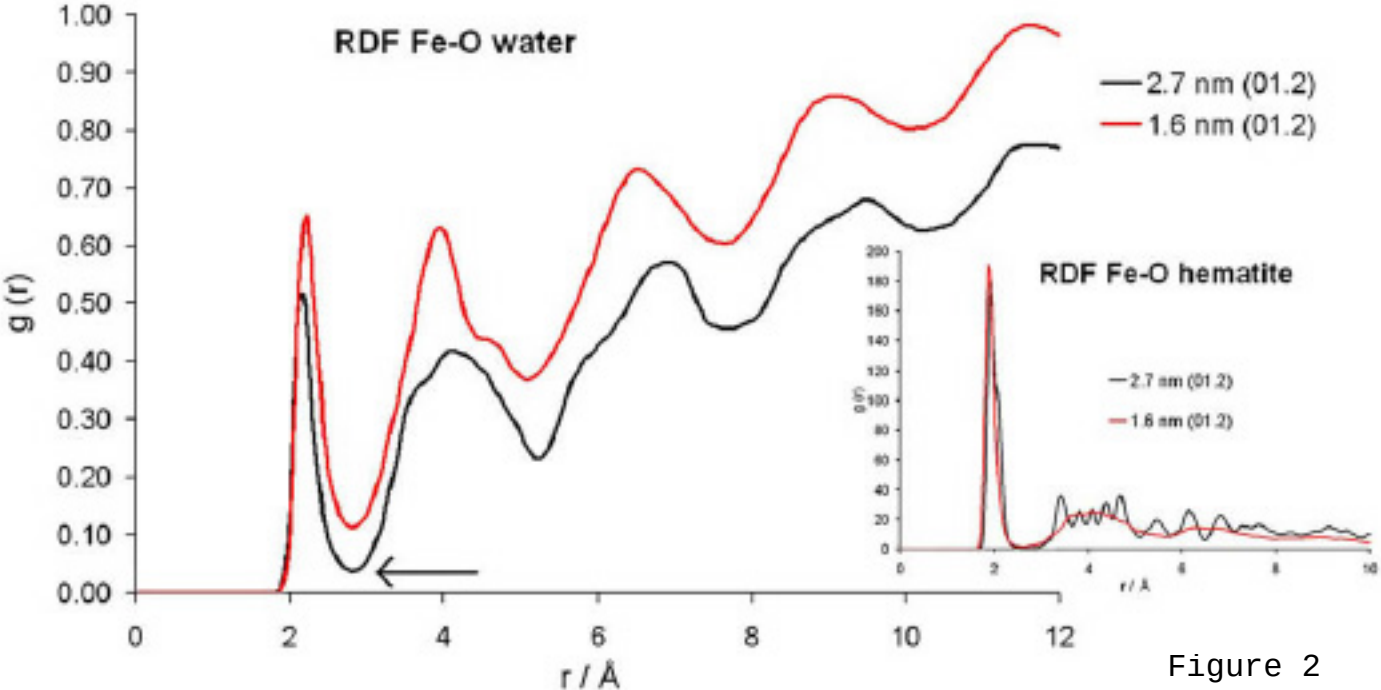
RDF Fe-O water
2.7 nm (01.2)
1.6 nm (01.2)
g (r)
r / Å
RDF Fe-O hematite
2.7 nm (01.2)
1.6 nm (01.2)
g (r)
r / Å

Figure 2

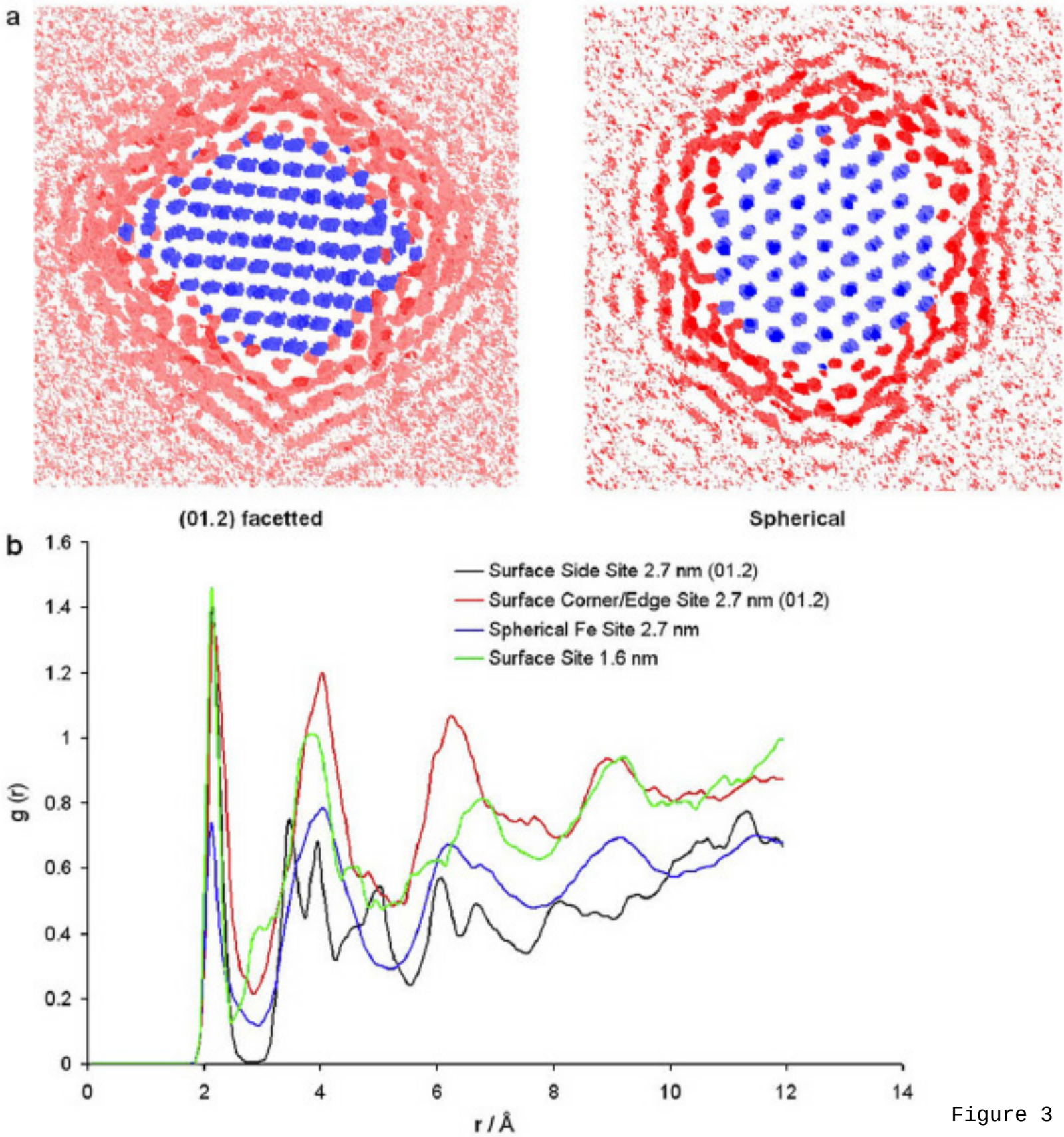
a
(01.2) facetted
Spherical
b
Surface Side Site 2.7 nm (01.2)
Surface Corner/Edge Site 2.7 nm (01.2)
Spherical Fe Site 2.7 nm
Surface Site 1.6 nm
g (r)
r / Å
0
0.2
0.4
0.6
0.8
1
1.2
1.4
1.6
0
2
4
6
8
10
12
14

Figure 3

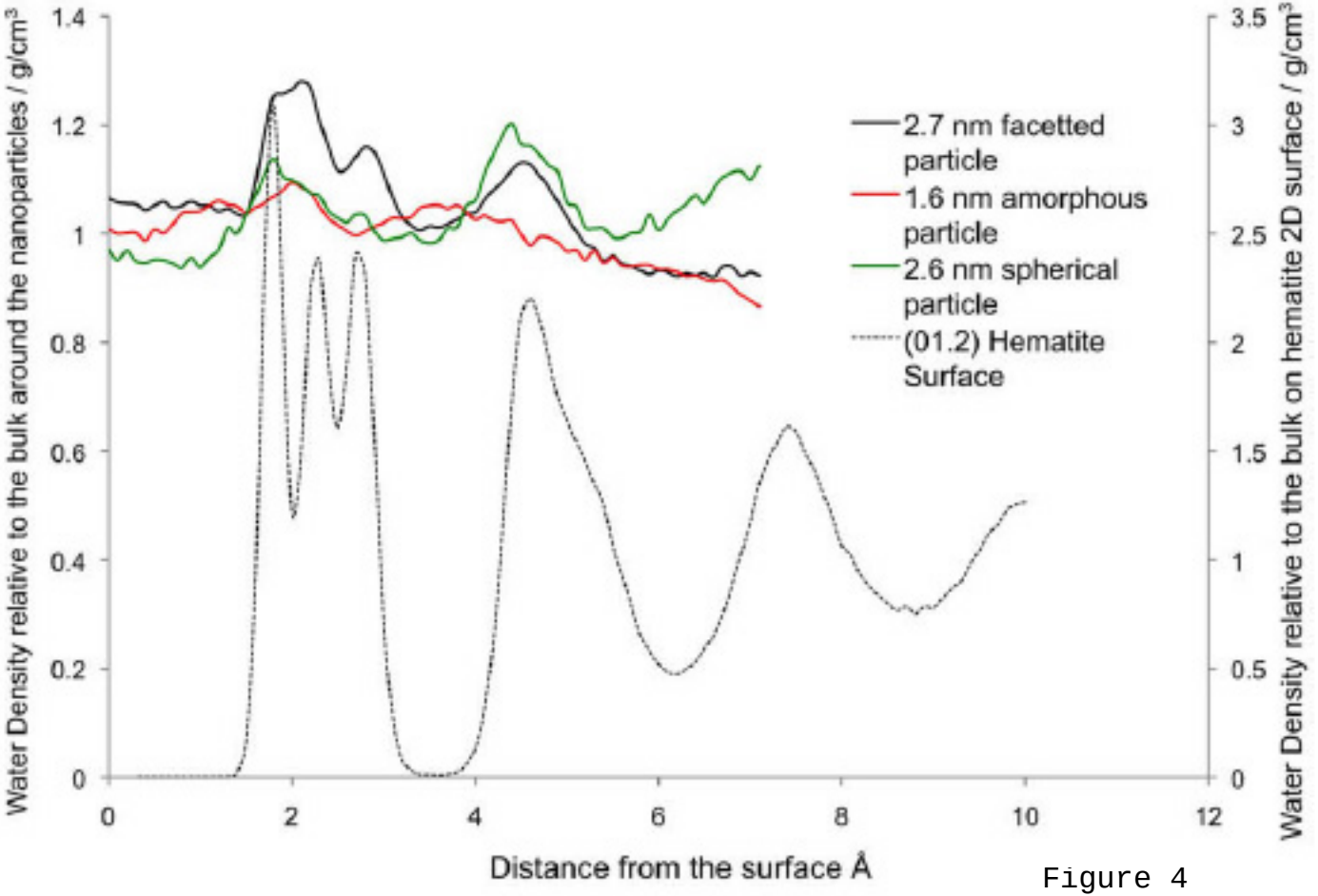
Water Density relative to the bulk around the nanoparticles / g/cm³
Water Density relative to the bulk on hematite 2D surface / g/cm³
Distance from the surface Å
2.7 nm facetted particle
1.6 nm amorphous particle
2.6 nm spherical particle
(01.2) Hematite Surface
0
0.2
0.4
0.6
0.8
1
1.2
1.4
0.5
1.5
2
2.5
3
3.5
2
4
6
8
10
12

Figure 4

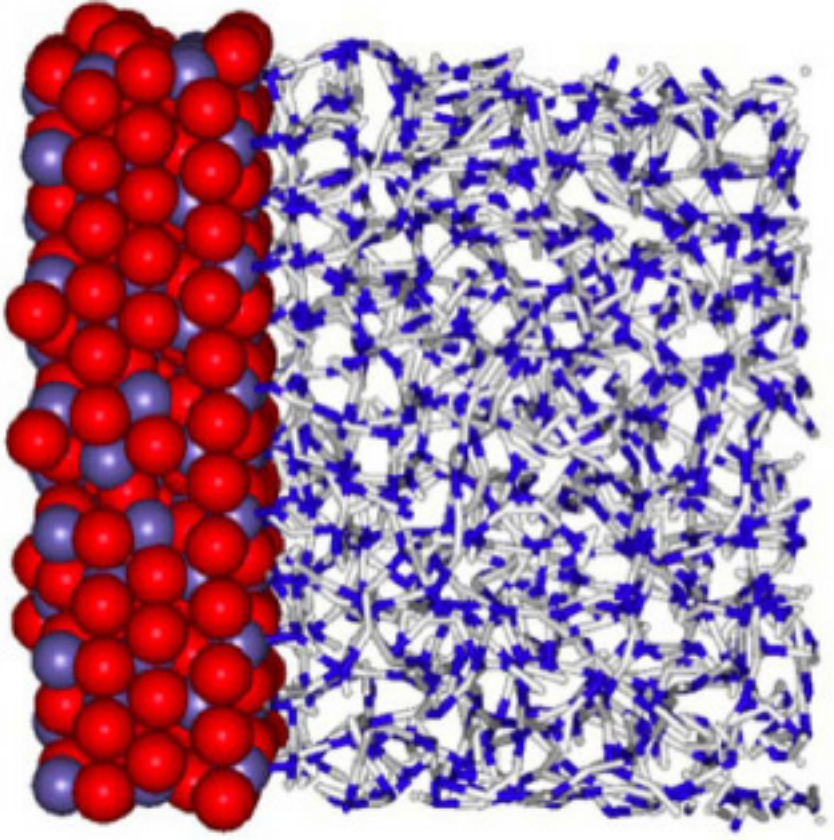

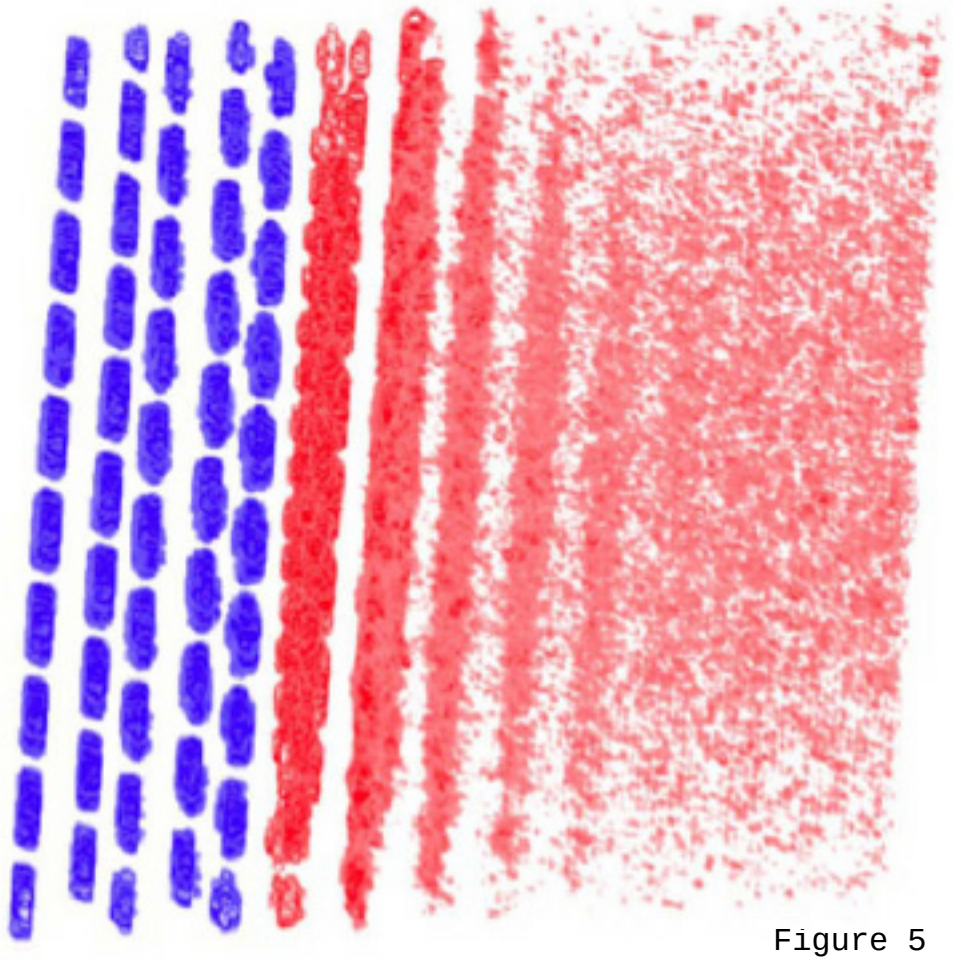

Figure 5